# THERMODYNAMIC AND CHEMICAL KINETIC ANALYSIS OF A 5 KW, COMPACT STEAM REFORMER – PEMFC SYSTEM

**Luis Evelio Garcia Acevedo**
Departamento de Engenharia Mecânica
Universidade Federal de Santa Catarina
Florianópolis/SC
evelio@labcet.ufsc.br

**Amir Antonio Martins Oliveira**
Departamento de Engenharia Mecânica
Universidade Federal de Santa Catarina
Florianópolis/SC
amirol@emc.ufsc.br

*Abstract. Here we present a thermodynamic and chemical kinetic analysis of the methane steam reforming for production of 5 kW of electrical power in a PEM fuel cell. The equilibrium analysis is based on the method of element potentials to find the state of minimum Gibbs free energy for the system and provides the equilibrium concentration of the reforming products. The objective of this analysis is to obtain the range of reforming temperature, pressure and steam-methane molar ratio that results in maximum hydrogen production subjected to low carbon monoxide production and negligible coke formation. The thermal analysis provides the heat transfer rates associated with the individual processes of steam production, gas-phase superheating and reforming necessary to produce 5 kW of electrical power in a PEM fuel cell and allows for the calculation of thermal efficiencies. Then, the chemical reaction pathways for hydrogen production in steam reforming are discussed and the available chemical, adsorption and equilibrium constants are analyzed in terms of thermodynamic consistency. This analysis provides the framework for the reactor sizing and for establishing the adequate operation conditions.*

*Keywords: methane steam-reforming, hydrogen, fuel cells, steam-reforming kinetics.*

## 1. Introduction

Hydrogen, as an energy source for mechanical and electrical decentralized or mobile power production, presents several advantages from the environmental point of view when compared to fossil fuels. Hydrogen can be burned directly into a combustion engine, but the main interest is in its use in fuel cells (FC), which promote an electrochemical clean efficient and quiet process for decentralized electric power generation. However, there are still problems of efficiency and scaling in the hydrogen production, storage, distribution and final use. Although hydrogen is the most abundant element in the universe, since it is extremely reactive, it is rarely found in nature in its standard form. Thus, it is necessary to spend energy to produce clean $H_2$ gas to be used as energy carrier. Therefore, a rational process for hydrogen production is important to avoid environmental degradation during synthesis. The ideal long-term source for hydrogen are the renewable sources such as biomass, wind, and solar. In developing countries, mostly in tropical or sub-tropical zones, such as in South America, the focus for hydrogen technology is the use of hydrogen obtained from renewable energy sources, including hydroelectricity, in decentralized power generation. However, in the short term, the use of fossil energy sources, specially the natural gas, appear as a promising technology promoting path. In Brazil, the increasing participation of natural gas in the energy matrix provides a convenient framework to develop a natural gas based hydrogen technology.

The industrial-scale steam reformers usually work at 700°C to 900°C and 20 to 40 bar with steam-methane ratios from 2:1 to 4:1. In typical reactors, the reacting mixture flows along 7.5 to 12 m long tubes with inner diameter between 7 to 13 cm (Twigg, 1989; Larmine e Dicks, 2000, Kordesh and Simader, 1996). The tubes are packed with catalyst pellets usually made of nickel impregnated alumina. Studies have addressed other catalytic metals (Berman et al., 2004), but nickel remains the most used industrially. Studies addressing the integration of the reformer to the PEM fuel cell (Mathiak et al., 2004) have reported that the main bottleneck of the system is the production of hydrogen gas with low carbon monoxide contents (below 50 ppm). Few works (Jorgenssen et al., 1995; Oklany et al., 1998) report the use of separation membranes in parallel with the reactor bed, thus allowing the hydrogen to seep through while it is produced. Palladium membranes have been found acceptable for most reactor conditions but are still expensive when compared to basic CO removal strategies (water gas-shift reactors and pressure-swing adsorption).

Even without addressing the final CO removal, issues remain regarding the proper sizing of small-scale compact reactors. Mathiak et al. (2004) developed an integrated compact reformer-PEMFC system for production of 2.5 kW of electrical power. The steam-reforming reactor was operated at 800°C and subsequent water-gas shift (WGS) reactors, a high temperature reactor operating at 400°C and a low temperature reactor operating at 200°C, were used. Their results

showed 64% global thermal efficiency at 500 W and 77% at 2500 W. The global thermal efficiency was defined as the ratio between the energy associated to $H_2$ at the reformer outlet and the total energy associated to $CH_4$, used for $H_2$ production and also to heat the reformer. The observed $H_2$, CO and $CH_4$ dry mole fraction in products was 79.5%, 54% and 53.5% at 500 W and 78%, 60% and 80.5% at 2500 W, respectively. Even with the use of high and low temperatures WGS reactors, the outlet CO concentrations were high and a final partial oxidation reactor (PrOx) was added. It is not clear whether the reforming reactor was controlled by kinetics or was sufficiently long and controlled by equilibrium. The answer to that requires a thermodynamic and a chemical kinetic calculation. Although the thermodynamic analysis is more straightforward, the kinetic analysis is not. Levent et al. (2003) report results for a micro flow steam-reforming reactor with 3 mm of diameter and up to 150 mm of length. Most of the reported literature values for chemical and adsorption kinetic constants are measured for temperatures under 600°C and pressures under 15 bar. Levent et al. (2003) note that these values of T and p are well below industry practice. They also notice that depending on T, P and the catalyst system used, not only the kinetic and adsorption parameters change, but also the chemical mechanism change, and a surface reaction may switch to a methane chemisorption or a CO desorption rate determining step. This makes the validation of chemical mechanisms hard to achieve and also makes it difficult to develop simulation for reactor design.

The main objective of this work is to analyze the thermodynamic constraints and the chemical kinetics of the methane stream reforming in order to obtain enough information to allow for the development of detailed heat and mass transfer simulations for a proper sizing and analysis of small-scale reactors (Garcia, 2006). To this objective, we present an analysis focused to operation conditions able to provide 5 kW of electrical power in a PEM fuel cell. A thermodynamic equilibrium analysis including six chemical species ($CH_4$, $H_2O$, $H_2$, CO, $CO_2$, C(S)) is performed to determine the adequate range for temperature, pressure and steam-methane ratio and to calculate the equilibrium concentration of products. The equilibrium analysis is based on the method of element potentials to find the state of minimum Gibbs free energy for the system and provides the equilibrium concentration of the reforming products. A thermal analysis provides the heat transfer rates associated with the individual processes of steam production, gas-phase superheating and reforming necessary to produce 5 kW of electrical power in a PEM fuel cell and allows for the calculation of thermal efficiencies. Then, the chemical reaction pathways for hydrogen production in steam reforming are discussed and the available chemical, adsorption and equilibrium constants are analyzed in terms of thermodynamic consistency. A reduced mechanism for the steam reforming including five chemical species ($CH_4$, $H_2O$, $H_2$, CO, $CO_2$) and three global reaction rates is assumed. These are the steam reforming (R1), the water gas shift reaction (R2) and the methanation reaction (R3):

$$CH_4 + H_2O \rightarrow CO + 3\,H_2, \qquad \Delta h_f (298\ K) = 206\ kJ/mol \qquad (R1)$$
$$CO + H_2O \rightarrow CO_2 + H_2, \qquad \Delta h_f (298\ K) = -41\ kJ/mol \qquad (R2)$$
$$CH_4 + 2\,H_2O \rightarrow CO_2 + 4\,H_2, \qquad \Delta h_f (298\ K) = 165\ kJ/mol \qquad (R3)$$

The methanation reaction is the global steam-reforming reaction to saturated products. Chemical kinetics and adsorption constants are obtained from the literature for nickel-alumina based catalysts. Comparison of the different available sets of parameters show the expected variation in behavior exhibited by different catalytic particles and reactor conditions. This analysis provides the framework for the reactor sizing and for establishing the adequate operation conditions. The solid carbon production is only predicted thermodynamically and is not taken into account in the chemical kinetic mechanism. Therefore, deactivation by coke formation is not explored.

## 2. THERMODYNAMIC ANALYSIS

This analysis aims at determining the product species equilibrium concentration and heat transfer rates as a function of the temperature, pressure and steam to methane ratio conditions. The chemical species selected as typical steam-reforming products are C(s), $CH_4$, CO, $CO_2$, $H_2$ and $H_2O$. Table 1 presents the range of parameters explored.

Table 1: Range of reactor pressure *P*, temperature *T* and steam to methane ratio *R* explored.

| Variable | Range |
|---|---|
| Pressure, *P* (atm) | 1, 1.2, 2, 4 |
| Steam to methane molar ratio, *R* (nond.) | 1, 1.5, 2, 4, 6, 10 |
| Temperature, *T* (°C) | 400, 450, 500, 550, 600, 650, 700, 750, 800, 850, 900 |

The STANJAN 4.0 code (Reynolds, 1995) was used to solve for the equilibrium states. This program uses the method of element potentials to find the state of minimum Gibbs free energy for the system, subjected to atom population constraints (Borman and Ragland, 1998). Unless noted, the results below are calculated for a 1 mol of CH4 basis.

Figure 1 presents the equilibrium number of moles of C(s) in the products as a function of the temperature for (a) different pressures and (b) different steam to methane molar ratios. It is observed in Fig 1(a) that a pressure increase causes a reduction in the C(s) equilibrium concentration. In Fig 1(b) it is observed that the equilibrium concentration of C(s) is negligible in all the temperatures calculated for steam to methane molar ratios $R$ greater than 1.5:1. We conclude that the equilibrium formation of C(s) is greatly reduced for pressures above 1.2 atm and steam to methane molar ratios greater than 1.5:1.



|     |     |
| :-: | :-: |
| (a) | (b) |
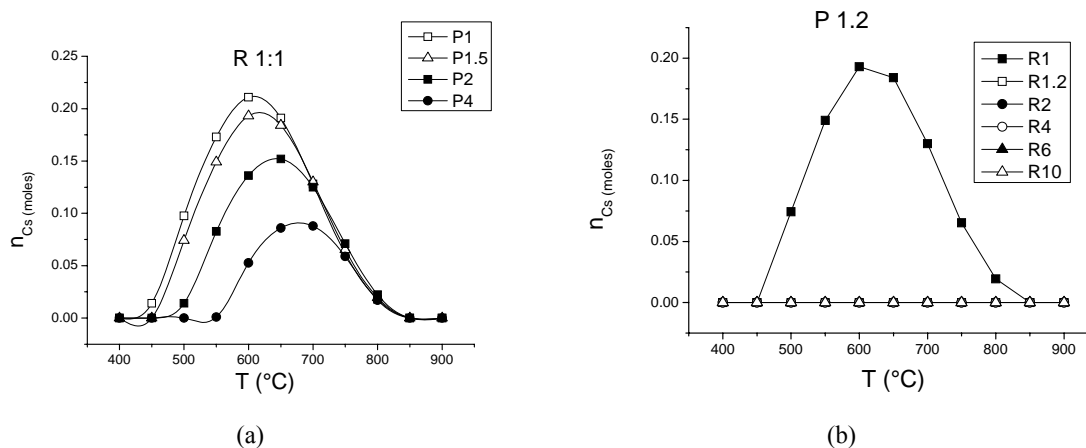
Figure 1: Equilibrium C(s) number of moles for 1 mol of $CH_4$ as a funtion of temperature for (a) different pressures and (b) different steam to methane molar ratios $R$.



|     |     |
| :-: | :-: |
| (a) | (b) |
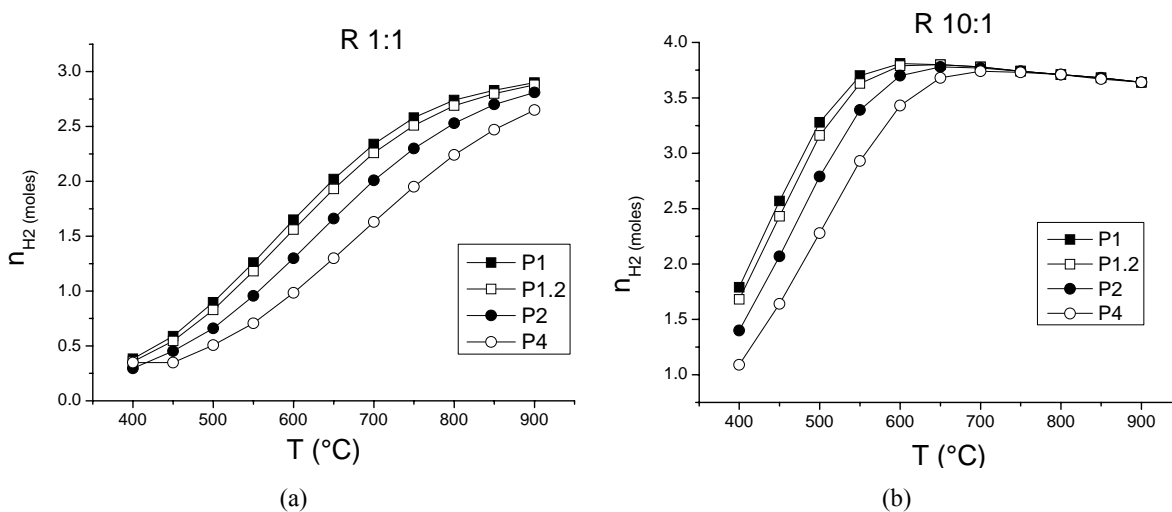
Figure 2: Equilibrium $H_2$ number of moles for 1 mol of $CH_4$ as a funtion of temperature for (a) steam to methane molar ratio $R$ =1 and (b) steam to methane molar ratio $R$ =10, for pressures from 1 atm to 4 atm.

Figure 2 presents the number of moles of hydrogen under equilibrium conditions as a function of temperature, for different values of pressure, for steam to methane molar ratio of (a) 1:1 and (b) 10:1. It is observed that the number of moles of hydrogen decreases as pressure is increased. The maximum stoichiometric number of moles of hydrogen as products is 4. For the 10:1 ratio, a maximum hydrogen production is achieved around 600 to 700°C, which is near 4. It will be shown later that excess water, however, reduces the overall thermal efficiency and a compromise between hydrogen production and energy efficiency must be reached.

Figure 3(a) presents the number of moles of hydrogen under equilibrium conditions as a function of temperature, for different values of steam to methane molar ratios, for a pressure of 1.2 atm. The curves indicate a rapid increase in hydrogen production as the steam to methane molar ratio $R$ increases from 1, followed by a smaller rate of increase for $R > 4$. For higher values of $R$, the hydrogen production peaks for temperatures above 600°C. Figure 3(b) presents the dry molar fraction of $H_2$ in equilibrium as a function of the steam to methane molar ratio for different temperatures. For $R > 4$ and $T > 600$°C the hydrogen mole fraction tend to the stoichiometric upper limit ($X_{H2} = 0.8$).

(a)                                                                                          (b)
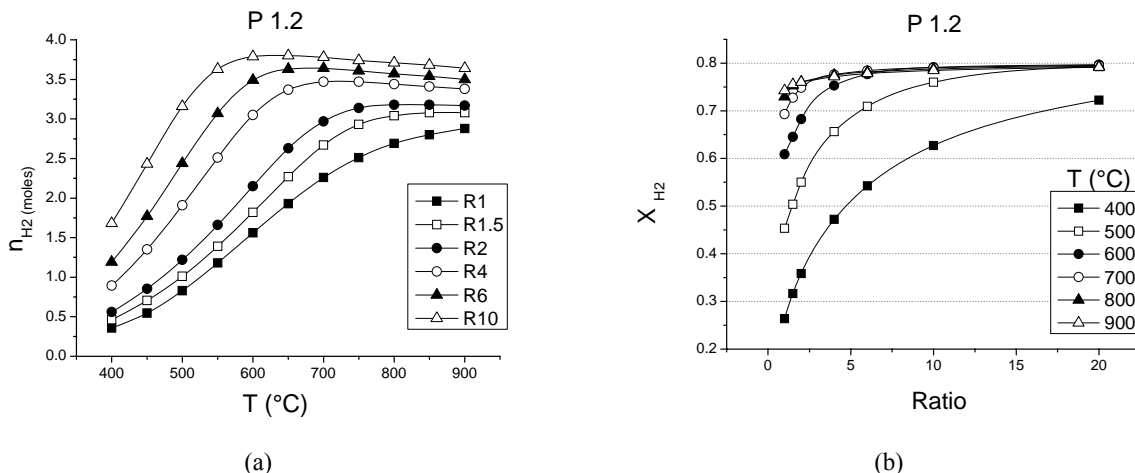
Figure 3: (a) Equilibrium $H_2$ number of moles for 1 mol of $CH_4$ as a funtion of temperature for steam to methane molar ratios from 1 to 10 and (b) Equilibrium dry $H_2$ mole fraction $X_{H2}$ as a function of the steam to methane molar ratio for temperatures from 400°C to 900°C.



(a)                                                                                          (b)
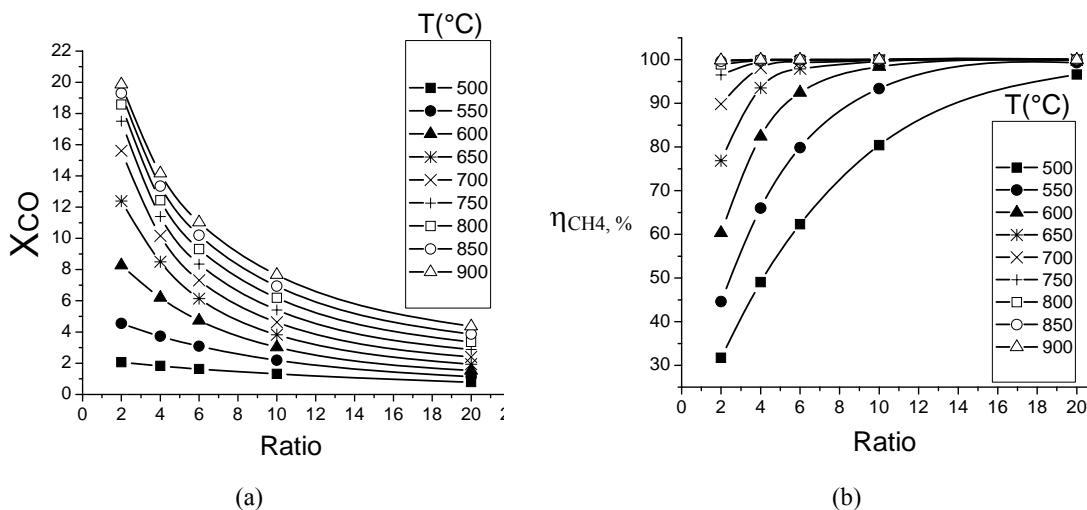
Figure 4 (a) Equilibrium dry mole fraction $X_i$ of CO as a function of steam to methane molar ratio and (b) equilibrium $CH_4$ conversion for temperatures from 400°C to 900°C and a pressure of 1.2 atm.

Figure 4(a) presents the equilibrium dry mole fraction of CO as a function of the steam to methane molar ratio for different temperatures at 1.2 atm. We note that the CO mole fraction decreases with the increase of the steam to methane ratio, as a result of the displacement of the equilibrium of the water-gas shift reaction to the direction of the $CO_2$ production. Since the formation of $CO_2$ is exothermic, higher temperatures favor the formation of CO. Figure 4(b) presents the equilibrium $CH_4$ conversion as a function of the steam to methane molar ratio for different temperatures at 1.2 atm. The conversion of $CH_4$ is defined as

$$\eta_{CH4} = \frac{n_{CH4\_inlet} - n_{CH4\_outlet}}{n_{CH4\_inlet}} \qquad (1)$$

We observe that an increase in temperature or an increase in steam to methane molar ratio results in conversion approaching 100%. Conversion is above 80% for R > 4 and T > 600°C. Comparing to Fig. 4(a) we note that the same conditions that provide better conversion also result in higher production of CO. A reasonable approach is to work with the highest possible conversion of $CH_4$, limited to materials and overall cost, while expecting the need for further CO removal operations, to lower concentrations under 50 ppm. This approach will be used to define the proper range for the reactor operating parameters.

Figure 5 presents the surface of equilibrium hydrogen number of moles as a function of temperature and steam to methane molar ratio for 1.2 atm. The level curves identify respectively 25%, 50% and 75% production of hydrogen when compared to the maximum stoichiometric value. The region identified with a circle bound by the limits of 650°C < *T* < 750°C and 4 < *R* < 6 results in hydrogen production above 80% of the maximum stoichiometric value. Other technological factors need to be considered to fix suitable operation parameters, like cost related to the vapor production, mechanical strength in high temperature, couplings, etc.. While most of these technological constraints are not addressed here, the energy spent for water vapor production can be easily taken into account, as follows.
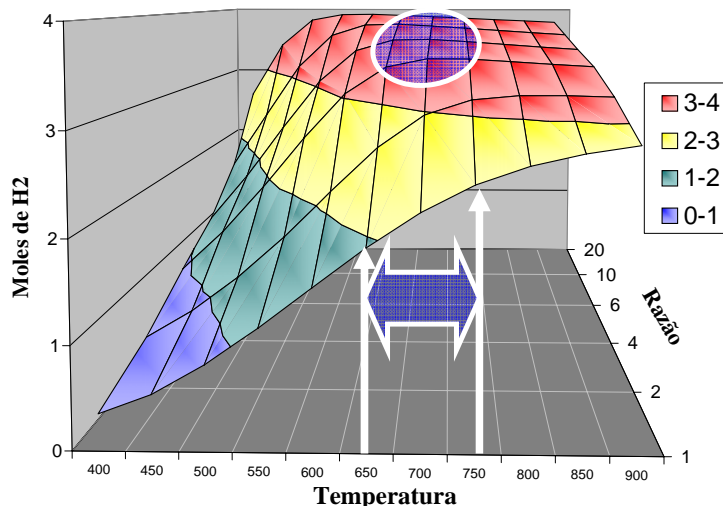


Figure 5: Equilibrium $H_2$ mole production for 1 mol of $CH_4$ as a funtion of temperature and steam to methane molar ratio. The circle identifies the range of possible best operation parameters.

The thermal analysis is performed assuming that the reformer feeds a PEM fuel cell with a 0.5 efficiency generating 5 kW of electrical power. This electrical power is typical of a common household that uses combustion for its heating necessities. The low FC efficiency is chosen to be a lower bound representative value (Mathiak et al., 2004; Larmine e Dicks, 2000, Kordesh and Simader, 1996)., whose effect, nonetheless, can be easily removed from the final results. The fuel cell efficiency $\eta_{cel}$ is related to the hydrogen flow by

$$\dot{n}_{H2\_el} = \frac{\dot{W}_{el}}{\Delta \overline{g}_f \eta_{Cel}}$$

(2)

where $W_{el}$ is the electrical power produced, $n_{H2\_el}$ is the hydrogen molar flux and $\Delta g_f$ is the molar Gibbs free energy change in the FC overall electrochemical reaction. It is assumed that the fuel cell is kept at a constant operation temperature of 80°C. At this temperature, $\Delta g_f$ = 226.1 kJ/mol (Larmine e Dicks, 2000).

The reformer, coupled to an external heat source fueled with methane and air (an auxiliary combustor), is integrated to the fuel cell. In this analysis, the fuel cell effluents are not reused for heating the reformer, all the heat generated by the auxiliary combustor, burning completely a stoichiometric mixture of methane and air, is used in the reformer and the reactor pressure is kept constant at 1.2 atm. We reinforce that no attempt was made to improve the overall thermal efficiency by using any form of internal heat recirculation or by simulating a cogeneration unit. The sole objective is to quantify the maximum heat transfer rates needed in each component.

Figure 6 presents a diagram with the main components of the system under analysis. The liquid water is fed at a mass flow rate ($m_w$) at the system pressure and undergoes liquid water heating ($Q_{w,l}$), phase change ($Q_{lv}$) and water vapor superheating ($Q_{w,v}$). Methane is fed at a mass flow rate ($m_f$). Part of this is fed at the system pressure and then superheated ($Q_{f,v}$). The superheated steam and methane are mixed and flow within the reactor where a heat transfer rate ($Q_r$) is absorbed. The remaining methane is used in an external combustion with air to provide the heat ($Q_r$) for the reforming reactor.

Figure 7(a) presents the water and methane volumetric flow rates (standard conditions) fed to the reforming unit for a constant equilibrium hydrogen flow rate at the reactor outlet (0.088 g/s is needed to produce 5 kW at 0.5 FC efficiency, which is equivalent to 3.87 m³/h), for different reactor temperatures, steam to methane molar rate R = 4:1 and pressure 1.2 atm. The methane volumetric flow rate $V_f$ includes both the methane fed to the reactor and the methane used in the external auxiliary heater (estimated based on the LHV of 49982 kJ/kg, assuming 100% heat transfer efficiency from flame to reactor). We observe that the minimum methane consumption occurs between 650°C and 700°C. We also note that the water volumetric flow rate for the production of 5 kW is only of the order of 67

cm³/min ≅ 4 liters/hour. Figure 7(b) presents the heat transfer rates to the system, identified in Fig. 6. The dominant heat transfer rates are used in the reforming and for water phase change. We observe that the increase in temperature results in higher methane conversion which results in higher heat transfer rate absorbed by the reactor. Since the water flow rate decreases when the reforming temperature in increased (Fig. 7a) the heat transfer rate for water heating and evaporation also decreases. This is followed by a small increase since the water flow rate also presents a small increase.
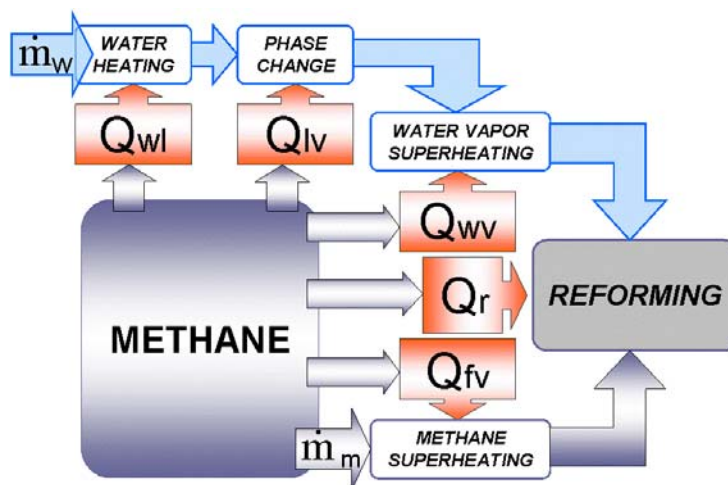


Figure 6: Diagram of the reforming unit showing the water heating, evaporation and superheating, methane superheating, mixing and reforming and the respective heat transfer rates (liquid water heating $Q_{w,l}$, water phase change $Q_{lv}$, water vapor superheating $Q_{w,v}$, methane superheating $Q_{f,v}$ and methane steam reforming $Q_r$).
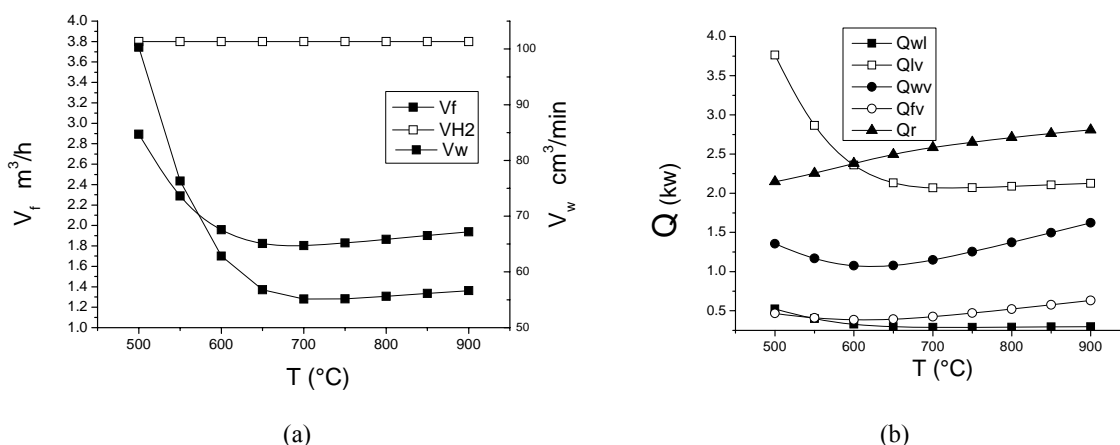


Figure 7 (a) Volumetric flow rate of hydrogen , methane (m³/h, on the left) and water (cm³/h on the right); and (b) heat transfer rates (kW) for the different steps during reforming (liquid water heating $Q_{w,l}$, water phase change $Q_{lv}$, water vapor superheating $Q_{w,v}$, methane superheating $Q_{f,v}$ and methane steam reforming $Q_r$) as a function of temperature, needed to generate 5 kW of electrical power in the FC system.

A global thermal efficiency of the fuel cell-reformer system can be defined as the electrical power generated divided by the total energy (LHV) associated with the methane flow, i.e.,

$$\eta = \frac{W_{ele}}{m_{CH4} \times LHV_{CH4}} \tag{3}$$

Figure 8 presents the variation of the global thermal efficiency of the fuel cell-reformer system with the temperature for steam to methane molar ratios R=2:1, R=4:1 and R=6:1. It can be observed that the efficiency reaches a maximum of approximately 30%. Since a 50% efficiency was assumed for the PEM fuel cell, and $\eta = \eta_{cel} \eta_{ref}$, this implies in a 60% efficiency for the reformer ($\eta_{ref} = 0.6$) producing equilibrium products. In the 650 – 700°C, a steam to methane molar ratio R = 4:1 results in the higher efficiency, although only marginally.
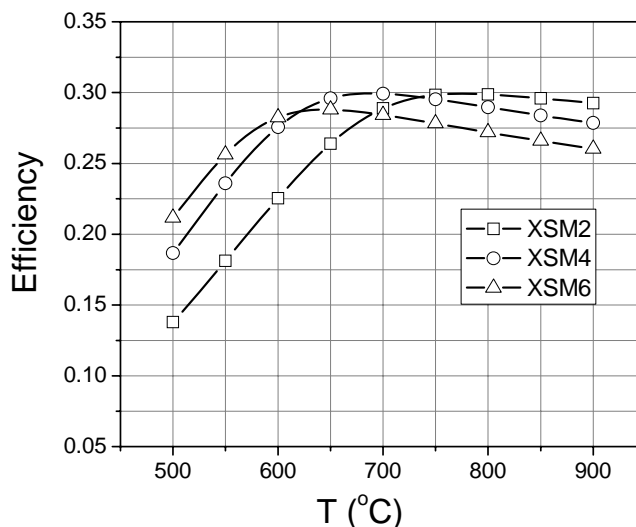
Figure 8: Global thermal efficiency η = η$_{cel}$ η$_{ref}$ of the reformer-fuel cell system at 1.2 atm. The curves are calculated for steam to methane molar ratios of 2:1, 4:1 and 6:1.

From the analysis above, Table 2 summarizes the operation conditions assumed for the reactor and the performance parameters that are obtained.

Table 2: Equilibrium operation and performance parameters for the reforming reactor operating at 1.2 atm, 700°C, R = 4:1 for a PEMFC producing 5 kW at $T_{cel}$ = 80°C, $\eta_{cel}$ = 0.5 (LHV$_{H2}$ = 119950 kJ/kg, LHV$_{CH4}$ = 49982 kJ/kg).

| Selected equilibrium operation parameters: | | | | | |
|---|---|---|---|---|---|
| $n_{H2}$, moles | $X_{H2}$ (dry basis) | $m_{H2}$, kg/s | $m_{CH4\ T}$, kg/s | $m_{H2O}$, kg/s | $\eta_{ref}$ |
| 3.47 | 0.776 | 8.7x10$^{-05}$ | 3.3x10$^{-04}$ | 9.2x10$^{-04}$ | 0.6 |

Although the thermodynamic analysis provides the thermodynamic bounds for hydrogen production, it says nothing about the speed of conversion and selectivity towards hydrogen. In the following, the chemical reaction pathways for hydrogen production in steam reforming are discussed and the available chemical, adsorption and equilibrium constants are analyzed in terms of thermodynamic consistency. This analysis provides the framework for the reactor sizing and for establishing the adequate operation conditions.

## 3. ANALYSIS OF THE SURFACE CHEMICAL REACTION RATE

Most reaction kinetic results available in the literature for alumina supported nickel catalysts point to a Langmuir-Hinshelwood kinetic mechanism. Xu and Froment (1989) developed a 13-step mechanism from which 3 reactions are selected assuming that the surface reaction is the rate limiting step which are the steam reforming (R1), the water gas shift reaction (R2) and the methanation reaction (R3), shown above. These three reactions divide the same active sites and for this reason the reaction rates share the same denominator which acts as an inhibitor. The elementary reaction rates can be written as

$$r_1 = \frac{\dfrac{k_{c1}}{p_{H_2}^{2.5}} \left( p_{CH_4} p_{H_2O} - \dfrac{p_{H_2}^3 p_{CO}}{K_{e1}} \right)}{\left( DEN \right)^2} \tag{4}$$

$$r_2 = \frac{\dfrac{k_{c2}}{p_{H_2}} \left( p_{CO} p_{H_2O} - \dfrac{p_{H_2} p_{CO_2}}{K_{e2}} \right)}{\left( DEN \right)^2} \tag{5}$$

$$r_3 = \frac{\dfrac{k_{c3}}{p_{H_2}^{3.5}} \left( p_{CH_4} p_{H_2O}^2 - \dfrac{p_{H_2}^4 p_{CO_2}}{K_{e3}} \right)}{\left( DEN \right)^2} \tag{6}$$

The inhibition term is:

$$DEN = 1 + K_{aCO} p_{CO} + K_{aH_2} p_{H_2} + K_{aCH_4} p_{CH_4} + \frac{K_{aH_2O} p_{H_2O}}{p_{H_2}} \tag{7}$$

In Eqs. (4) to (7), $p_i$ is the species i partial pressure (Pa); $k_{ci}$ is the chemical kinetic constant and $K_{ei}$ is the chemical equilibrium constant for reactions R1, R2 and R3; and $K_{ai}$ is the species i adsorption constant. The values of the activation energy satisfy Arrhenius equations and the enthalpies satisfy van´t Hoff equations. Then, for the kinetic constant we have,

$$k_{ci} = A\left( k_{ci} \right) \exp\left( -\frac{E_i}{RT} \right) \tag{8}$$

where

$$A\left( k_{ci} \right) = k_{ci,T_r} \exp\left( \frac{E_i}{RT_r} \right) \tag{9}$$

For the adsorption constant we have,

$$K_{a j} = A\left( K_{a j} \right) \exp\left( -\frac{\Delta H_j}{RT} \right) \tag{10}$$

where

$$A\left( K_{a j} \right) = K_{a j,T_r} \exp\left[ \frac{\Delta H_j}{RT_r} \right] \quad j = 1, 2, 3, 4 \tag{11}$$

and $R$ is the universal gas constant (8314.172 J/kmol.K), $A\left( k_i \right)$ is the pre exponential coefficient for the kinetic constant, $E_i$ is the activation energy, $A\left( K_{a j} \right)$ is the pre exponential coefficient for the adsorption constant, and $\Delta H_j$ is the adsorption enthalpy change and Tr is the reference temperature . The parameters used are such that the reaction rates $r_i$ for reactions R1, R2 and R3 return in kmol/kgcat.s. The equilibrium constants can be calculated from thermodynamic tables, such as in STANJAN, or curve fitted, such as presented by Twigg (1989) and other authors. As shown below, not all the expressions presented are thermodynamically consistent.

From the chemical kinetic mechanism (reactions R1 to R3), the formation and destruction rates of the chemical species are calculated from

$$
\begin{aligned}
r_{CH_4} &= -\left( r_1 + r_3 \right) \\
r_{H_2O} &= -r_1 - r_2 - 2r_3 \\
r_{H_2} &= 3r_1 + r_2 + 4r_3 \\
r_{CO} &= r_1 - r_2 \\
r_{CO_2} &= r_2 + r_3
\end{aligned}
\tag{12}
$$

Xu and Froment (1989) XF tested the reaction mechanism in the range of 300-574°C. In their experiments, there was no diffusion limitation. Several other authors, using this same reaction mechanism, have proposed sets of constants that provide predictions that match their experimental results. From these, the constants reported by Elnashaie et al. (1990) EAU; Adris, et al. (1996) ALG ; Barbieri and Di Maio (1997) BD; Xiu et al. (2002) XSL; Nielsen et al. (2003) NK and Hoang et al. (2005) HCD, were used and the results were compared. Table 2 summarizes the reaction conditions reported in the references. In Table 2, R stands for the steam to methane molar ratio, $\rho_{cat}$ is the catalyst concentration, $\rho_p$ is the pellet density, $\varepsilon_p$ is the pellet porosity and $d_p$ is the pellet diameter.

The equilibrium constants were calculated using the expressions provided by the references and was also obtained from STANJAN. Figure 9 presents the variation of the equilibrium constant for the methane steam reforming $K_{e1}$ calculated from the constants provided by the references listed above. A group of references (XF-GPB-EAU-ALG-XSL) provide results similar to STANJAN, while functions reported by other authors deviate substantially. A better agreement between the references and STANJAN is observed in Fig. 10 for the equilibrium constant for the water gas shift reaction $K_{e2}$ and for the methanation reaction $K_{e3} = K_{e1} K_{e2}$ It is worth noting that $K_{e2}$ (WGS reaction R2) favors reactants as the temperature increases above approximately 1000 K, as expected from Le Chatelier principle.

Table 2 Summary of conditions for the references selected.

| Reference | Conditions | | | |
|---|---|---|---|---|
| | $T$, ºC | $P$, MPa | $R$ | Catalyst |
| Xu and Froment (1989), XF | 300-574 | 0.3, 0.5, 1, 1.5 | 3, 5 | Ni/MgAl$_2$O$_4$ Spinel, 15,2% wt Ni, BET 58 m$^2$/g |
| Elnashaie et al. (1990), EAU | 526-926 | 0.1 - 1.5 | 1, 2, 3, 6 | Ni/Al$_2$O$_3$, $\rho_{cat}$ = 1225 kgcat/m$^3$ |
| Adris et al. (1996), ALG | 541, 600, 700, 800 | 0.64, 1.5 | 3.5 | Ni/Al$_2$O$_3$, $\varepsilon_p$ = 0.5 |
| Barbieri and Di Maio (1997), BD | 300, 500 | 0.136 | 3 | Comercial Ni/Al$_2$O$_3$ |
| Xiu et al. (2002), XSL | 450, 650 | 0.125, 0.445 | 6 | Comercial Ni/Al$_2$O$_3$ pellet, $\rho_{cat}$ = 233.3 kgcat/m$^3$, $\varepsilon_p$ = 0.5, $d_p$ = 3 mm, $\rho_p$ = 1550 kg/m$^3$ |
| Nielsen et al. (2003), NK | 300-574 | 0.3, 0.5, 1, 1.5 | 3, 5 | Ni/MgAl$_2$O$_4$ Spinel, 15,2% wt Ni, BET 58 m$^2$/g |
| Hoang et al. (2005), HCD | 500, 800 | 0.15 | 2 - 5 | Ni-0309/S, 9.8% wt Ni, BET 155 m$^2$/g |

A relative deviation between the equilibrium constants Ke1 e Ke2 obtained from the expressions reported by the references in respect to the values calculated from STANJAN (Deviation = $1 - K_{ei} / K_{ei\_STANJAN}$) is calculated. The results (not shown here) indicate that, when compared to STANJAN, the curve fit used by XLS return values that are within 0.5% and also presented a smoother variation in the temperature range from 500 to 900ºC. These expressions where originally taken from Twigg (1989). They are recommended for use in simulations and are reproduced here:

$$K_{e1} = \frac{1}{\exp\left(Z\left(Z\left(Z\left(0,2513Z - 0,3665\right) - 0,58101\right) + 27,1337\right) - 3,2770\right)}$$

$$K_{e2} = \exp\left(Z\left(Z\left(0,63508 - 0,29353Z\right) + 4,1778\right) + 0,31688\right) \tag{13}$$

$$K_{e3} = K_{e1}K_{e2}$$

where $Z = \left(1000/T\right) - 1$.
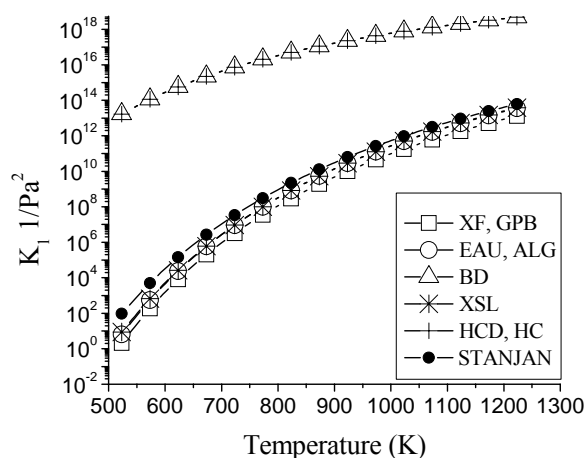
Figure 9 Methane steam-reform reaction equilibrium constant $K_{e1}$ as a function of temperature using the constants and functions reported in the references and as calculated from STANJAN.



(a)

(b)
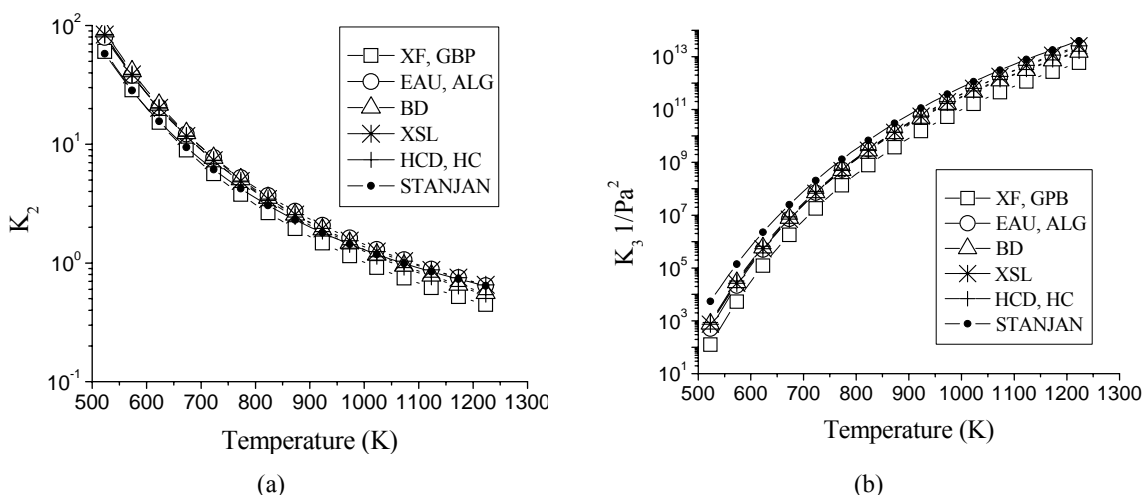
Figure 10 (a) Water gas shift reaction constant $K_{e2}$ and (b) methanation reaction equilibrium constant $K_{e3}$ as a function of temperature using the constants and functions reported in the references and as calculated from STANJAN.

Table 3 Kinetic and adsorption parameters converted to homogeneous SI units from the values reported in the references cited above.

| Reference | | Kinetic constants | | | Adsorption constants | |
|---|---|---|---|---|---|---|
| | | A(kci) [(1)] | Ei, J/kmol | | A(Kaj) [(2)] | ΔHj, J/kmol |
| Xu and Froment (1989), XF, [23] | R1 | 3.736E+14 | 2.401E+08 | CO | 8.122E-10 | -7.065E+07 |
| and Nielsen et al. (2003), NK, [30] | R2 | 5.360E-03 | 6.713E+07 | H2 | 6.040E-14 | -8.292E+07 |
| | R3 | 9.019E+13 | 2.439E+08 | CH4 | 6.563E-09 | -3.828E+07 |
| | | | | H2O | 1.770E+05 | 8.868E+07 |
| Elnashaie et al. (1990), EAU, [24] | R1 | 2.636E+15 | 2.401E+08 | CO | 8.230E-11 | -7.065E+07 |
| and Adris et al. (1996), ALG, [25] | R2 | 1.219E-03 | 6.713E+07 | H2 | 6.120E-15 | -8.290E+07 |
| | R3 | 6.361E+14 | 2.439E+08 | CH4 | 6.650E-10 | -3.828E+07 |
| | | | | H2O | 1.770E+05 | 8.868E+07 |
| Barbieri and Di Maio (1997), BD, [26] | R1 | 3.711E+14 | 2.401E+08 | CO | 8.230E-10 | -7.065E+07 |
| | R2 | 5.431E-03 | 6.713E+07 | H2 | 6.120E-14 | -8.290E+07 |
| | R3 | 8.961E+13 | 2.439E+08 | CH4 | 6.650E-09 | -3.828E+07 |

| | | | | H2O | 1.770E+05 | 8.868E+07 |
|---|---|---|---|---|---|---|
| Xiu et al. (2002), XSL, [29] | R1 | 1.629E-05 | 2.401E+08 | CO | 4.038E-04 | -7.065E+07 |
| | R2 | 2.072E-08 | 6.713E+07 | H2 | 2.921E-07 | -8.290E+07 |
| | R3 | 1.939E-06 | 2.439E+08 | CH4 | 1.768E-06 | -3.828E+07 |
| | | | | H2O | 4.152E-01 | 8.868E+07 |
| Hoang et al. (2005), HCD, [33] | R1 | 8.000E+07 | 2.095E+08 | CO | 8.004E-10 | -3.665E+07 |
| | R2 | 1.489E-06 | 7.020E+07 | H2 | 6.958E-14 | -7.023E+07 |
| | R3 | 1.892E+05 | 2.115E+08 | CH4 | 1.969E-08 | -8.255E+07 |
| | | | | H2O | 1.680E+04 | 8.577E+07 |

Obs.: Units:

(1) Kinetic constants:  (2) Adsorption constants:

R1  (kmol/kgcat-s)(Pa^0.5)  CO  1/Pa

R2  (kmol/kgcat-s)(Pa^-1)  H2  1/Pa

R3  (kmol/kgcat-s)(Pa^0.5)  CH4  1/Pa

  H2O  adm.

    Table 4 presents the kinetic and adsorption parameters converted to homogeneous SI units from the values reported in the references cited above. We note that although the same kinetic mechanism is assumed, since their experiments were performed using different catalysts and supports, the reported parameters are different, reflecting different catalytic reaction rates. Figure 11 presents the kinetic constants and Figure 12 presents the adsorption constants calculated from the set of parameters provided by the authors cited above. In particular, the catalytic reactor of Hoang et al. (2005) HCD is considerably less reactive than the reactors reported by the other references.



(a)



(b)



(c)
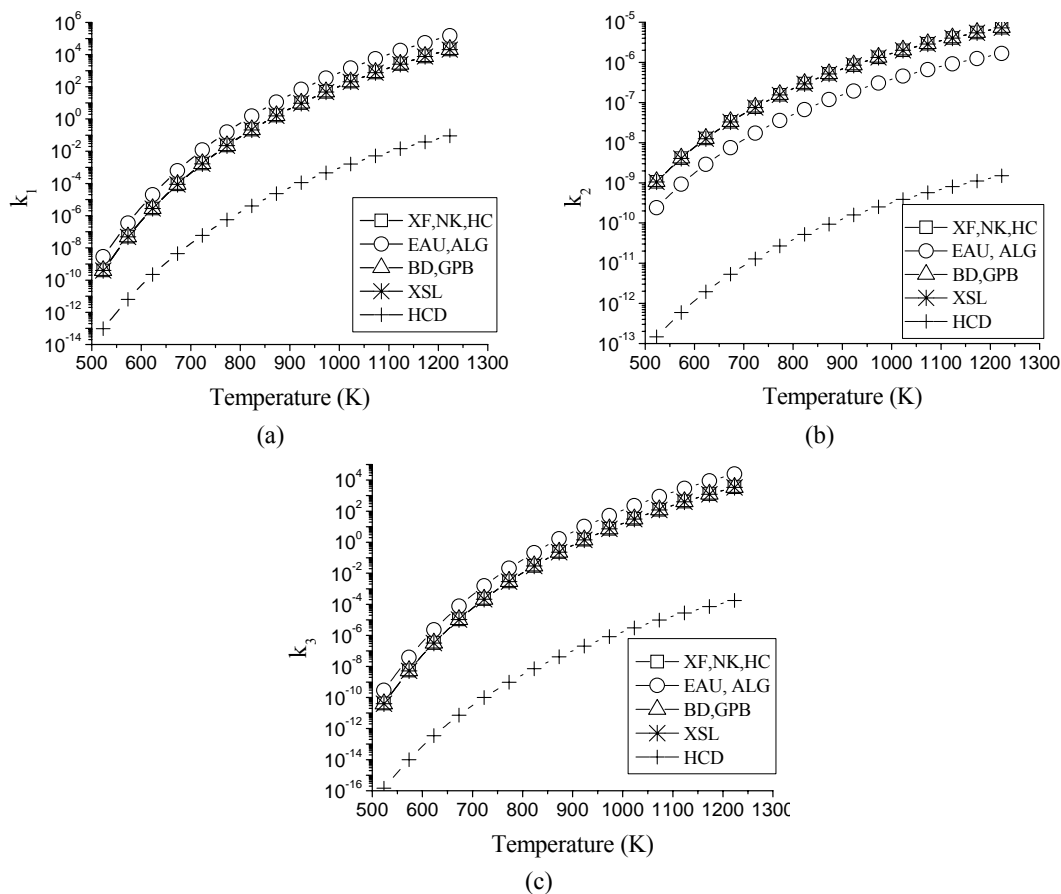
Figure 11: Kinetic constants for (a) steam reforming reaction kc1, (b) water gas shift reaction kc2 and (c) methanation reaction $k_{c3}$, as a function of temperature, at a constant pressure of 1.2 atm, calculated using the kinetic parameters listed in the references.
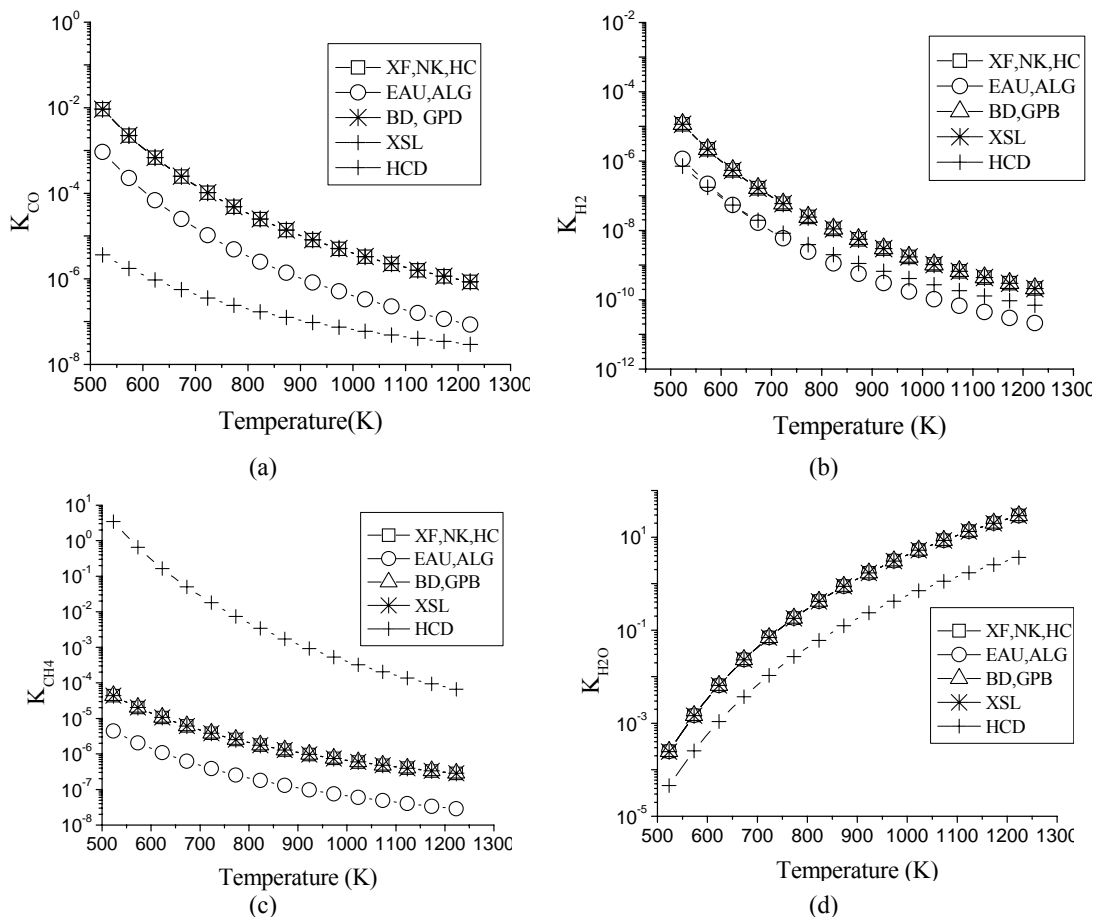
Figure 12 Adsorption constants of the species at a constant total pressure of 1.2 atm as a function of the temperature for (a) CO, $K_{CO}$ ;(b) $H_2$, $K_{H2}$; (c) $CH_4$, $K_{CH4}$; (d) $H_2O$, $K_{H2O}$; using the adsorption parameters listed in the references.

## 4. CONCLUSION

Here, a thermodynamic equilibrium analysis including six chemical species ($CH_4$, $H_2O$, $H_2$, CO, $CO_2$, C(S)) is performed to determine the adequate range for temperature, pressure and steam-methane ratio and to calculate the equilibrium concentration of products. The equilibrium analysis is based on the method of element potentials to find the state of minimum Gibbs free energy for the system and provides the equilibrium concentration of the reforming products. A thermal analysis provides the heat transfer rates associated with the individual processes of steam production, gas-phase superheating and reforming necessary to produce 5 kW of electrical power in a PEM fuel cell and allows for the calculation of thermal efficiencies. Then, the chemical reaction pathways for hydrogen production in steam reforming are discussed and the available chemical, adsorption and equilibrium constants are analyzed in terms of thermodynamic consistency. A reduced mechanism for the steam reforming including five chemical species ($CH_4$, $H_2O$, $H_2$, CO, $CO_2$) and three global reaction rates is assumed. These are the steam reforming, the water gas shift reaction and the methanation reaction.

The thermodynamic analysis allowed to select conditions adequate for steam-reforming in compact small-scale reactors which are 1.2 atm, 700°C and steam to methane molar ratio of 4:1. For a PEMFC producing 5 kW at Tcel = 80oC and assuming a FC efficiency $h_{cel}$ = 0.5, the reformer would require 9.2x10-4 kg/s of methane and 3.3x10-4 kg/s of water to produce 8.7x10-5 kg/s of hydrogen. The equilibrium reformer efficiency at these conditions is estimated in 0.6.

The chemical kinetic analysis revealed the large variation found in chemical kinetic parameters available in the literature. These reflect the different catalytic systems developed. As a basis for theoretical predictions and reactor sizing, the set of constants provided by Xu and Froment (1989) could be utilized. We reinforce, however, that the use of this set of constants does not guarantee a safe reactor sizing, since, as shown above, the reaction rates depend strongly on the catalytic metal, support and preparation method used for each catalytic system in particular.

In a follow-up article (Garcia and Oliveira, 2006), the thermodynamic and kinetic results presented above are used as a basis for a heat and mass transfer simulation of a monolith type steam-reforming reactor.

**Aknowledgements:**

**5. REFERENCES**

BERMAN, A., KARN, R. K. and EPSTEIN. M.; Kinetic of Steam reforming of methane on Ru/Al2O3 catalyst promoted with Mn oxides. Applied catalysis A:. General, v. 282, p. 73-83, 2004.

BORMAN, G. L. and RAGLAND, K. W., Combustion Engineering, McGraw-Hill, Boston, EUA, 1998.

GALLUCCI, Fausto. PATURZO, Luca. BASILE, Angelo. A simulation study of the steam reforming of methane in a dense tubular membrane reactor. . International Journal of hydrogen energy. v. 129, p. 611-617. Italy. 2003.

GARCIA, L. E. A., Simulação e análise de um reator de reforma de metano para a produção de hidrogênio. Dissertação de Mestrado, Programa de Pós-Graduação em Engenharia Mecânica, Universidade Federal de Santa Catarina, 2006.

GARCIA, L. E. A. and OLIVEIRA, A. A. M., Multi-scale modeling of the heat and mass transfer in a monolithic methane steam reformer for hydrogen production, Proceedings of ENCIT 2006, ABCM, Curitiba, Brazil, Dec. 5-8, 2006.

HOANG. D.L, CHAN.S.H; Modeling of a catalytic autothermal methane reformer for fuel cell application. Applied Catalysis A. General. v. 268, p. 207-216. Singapore. 2004.

HOANG. D.L, CHAN.S.H, DING.O.L; Kinetic and modelling study of methane steam reformer over sulfide nickel catalyst on a gamma alumina support. Chemical Engineering Journal. v. 112, p. 1-11, 2005.

HOU, Kaihu. HUGHES, Ronald; The kinetics of methane steam reforming over a Ni/α-Al2O catalyst. Chemical Engineering Journal v. 82, p. 311-328. . UK. 2000 (2001).

JORGENSEN, S. L., NIELSEN, P. E. H. and LEHRMANN, P. Steam reforming of methane in a membrane reactor. Catalysis Today. v. 25, p. 303-307, 1995.

KORDESCH, K. and SIMADER, G., Fuel Cells and Their Applications, VCH, 1996.

LARMINIE, J. and DICKS, A., Fuel Cell System Explained; 2000.

LEVENT, M., BUDAK G. and KARABUTUT A.; Estimation of concentration and temperature profiles for methane-steam reforming reaction in a porous catalyst. Fuel Processing Technology, v. 55, p. 251-263, 1998.

LEVENT, M., GUNN, D. J. and EL-BOUSIFFI, M. A., Production of hydrogen-rich gases from steam reforming of methane in an automatic catalytic microreactor, Int. J. Hydrogen Energy, v. 28, pp. 945-959, 2003.

MATHIAK, J., HEINZEL, A., ROES, J., KALK, Th., KRAUS, H. and BRANDT, H., Coupling of a 2.5 kW steam reformer with a 1 kWel PEM fuel cell, Journal of Power Sources, v. 131, pp. 112-119, 2004.

MATSUMARA, Y. and NAKAMORI, T.; Steam reforming of methane over nickel catalysts at low reaction temperature. Applied Catalysis A: v. 258, p. 107-114, 2003.

NIELSEN, M. P. and KAER, S. K.; Modeling a PEM fuel cell natural gás reformer, Proceedings of ECOS 2003, pp. 929-937. 2003.

OKLANY, J. S., HOU, K. and HUGHES, R., A simulative comparison of dense and microporous membrane reactors for steam reforming of methane. Applied Catalysis A: General, v. 170, p. 13-22, 1998.

PEDERNERA, M. N., PINA, J., BORIO, D. O., BUCALÁ, V., Use of a heterogeneous two-dimensional model to improve the primary steam reformer performance, Chemical Engineering Journal, v. 94, pp. 29-40, 2003.

REYNOLDS, W. S., STANJAN Chemical Equilibrium Solver, Version 4.0, Stanford, USA, 1995.

TWIGG, V. M., Catalyst Handbook. 2nd edition, Wolfe Publishing Ltd, Cleveland, 1989.

XIU, G., SOARES, J. L. and RODRIGUES, A. E., Simulation of five-step one-bed sorption-enhanced reaction process. AIChE Journal. v. 48, n.12, p. 2817-2832, 2002.

XIU, G., LI, P. and RODRIGUES, A. E., Adsorption-enhanced steam-methane reforming with intraparticle-diffusion limitations, Chemical Engineering Journal, v. 95, pp. 83-93, 2003.

XU, J. and FROMENT, G. F., Methane steam reforming, methanation and water-gas shift: I. Intrinsic kinetics, AIChE Journal, v. 35, n.1, pp. 88-96, 1989.